Quarterly Progress Report 2

Radar Studies of the Moon

15 May 1967

Issued 31 May 1967

Prepared for the U.S. National Aeronautics and Space Administration under Contract NSR 22-009-106 by

Lincoln Laboratory

MASSACHUSETTS INSTITUTE OF TECHNOLOGY

Lexington, Massachusetts

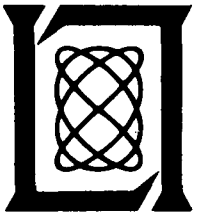

FOREWORD

This report is the sixth in a series of quarterly progress reports under Contract NSR 22-009-106 between the National Aeronautics and Space Administration and Lincoln Laboratory. Previous quarterly progress reports are referred to as QPR (1966:1) through QPR (1967:1). It is intended that this will be the last quarterly progress report; the final project report will be issued on 31 August 1967.

Section I of this report describes the progress which has been made in the mapping at 3.8 cm. Most of the area within 10° of the lunar equator has now been observed, and much of the data have been converted to intensity maps. Section II discusses some further studies of the supersynthesis technique, primarily in anticipation of its use for future polarization studies at 23-cm wavelength. Section III describes advances in the 8-mm radar observations.

CONTENTS

I. HIGH-RESOLUTION 3.8-CM REFLECTIVITY MAPPING

At the end of the current reporting period, the entire region of the lunar surface lying between 10° latitude north and south and 70° longitude east and west had been observed at 3.8 cm using the Haystack radar. In addition, several small areas lying outside this region of primary concern had been observed because of some special interest connected with them. The Fourier analysis of these observations has been largely completed, but the final task of producing maps has been delayed so that all the maps will be of identical format.

A number of improvements in the overall system have been introduced in the last three months. In the mapping program, it is now possible to accommodate a run having simultaneously 200 samples in delay and 256 in Doppler. The display program has also been modified to present an optical image having 200 by 200 resolution elements. The combination thus permits retention of the full data content of a given run under all conditions, and maximizes the operating efficiency. An example of data taken, processed, and displayed using these new programs is shown in Fig. 1.

A second improvement has been the construction of filters to permit the use of 5-μsec transmitted pulses and sampling intervals. The short pulses were not used as part of the broad survey of the equatorial regions except in several of the observations taken near the center of the disk where the resolution otherwise would have been very poor. However, they have been used to study the eight most recently selected possible Apollo lunar landing sites in as much detail as possible. A mapping run using the 5-μsec resolution has also been taken of the crater Tycho and is shown in Fig. 2. Figures 1 and 2 were obtained within an hour of each other on 21 March 1967 using 10- and 5-μsec delay resolutions, respectively, so that a direct comparison of the improvement may be made. Comparison may also be made with Fig. 6 of QPR (1967:1) which was taken on 21 December 1966. Because of a substantial difference in the location of the subradar point on the two dates, the improvement afforded by the shorter pulse was not as dramatic as it would be otherwise. Nevertheless, the resolution maintained in Fig. 2 is only slightly worse than 1 km.

Finally, the ability to map the output in Mercator projection has been added. Thus, after suitable enlargement it should be relatively easy from the final radar maps to construct overlays which will permit direct comparison with the corresponding Lunar Aeronautical Chart. It is expected that the option of mapping in Lambert projection also will be included shortly.

Figure 3 is included to demonstrate the high resolution of the radar mapping technique for regions near the lunar limb. The data obtained in this region are particularly useful, of course, because of the difficulty in obtaining ground-based optical measurements of equivalent resolution. Other than to test the method in this region of the lunar surface, however, no systematic mapping is presently planned.

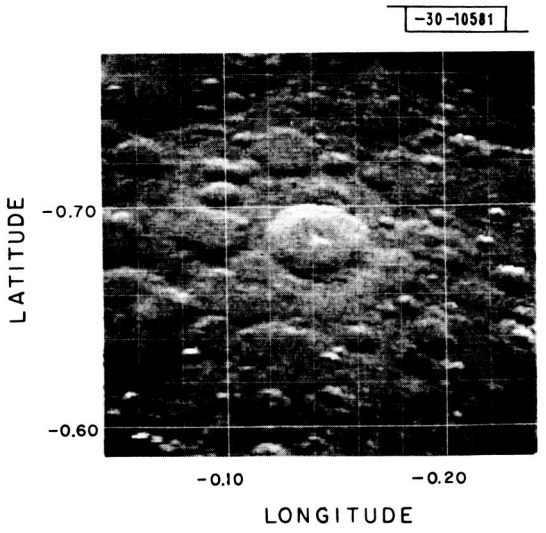

Fig. 1. Lunar surface in vicinity of crater Tycho using 10-μsec resolution as mapped by Haystack radar at 3.8-cm wavelength. Coordinates used here are selenographic Cartesian, normalized to lunar radius. Thus, a small grid square is 0.02 by 0.02 and resolution is 0.001 by 0.001 or approximately 2 km.

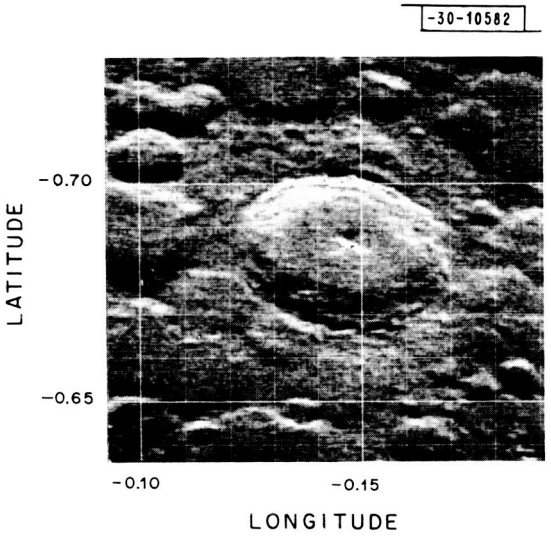

Fig. 2. Radar map of crater Tycho using 5-μsec resolution taken shortly after map shown in Fig. 1. Here, a small grid square is 0.01 by 0.01 lunar radius units and resolution is 0.0005 by 0.0005 or approximately 1 km.

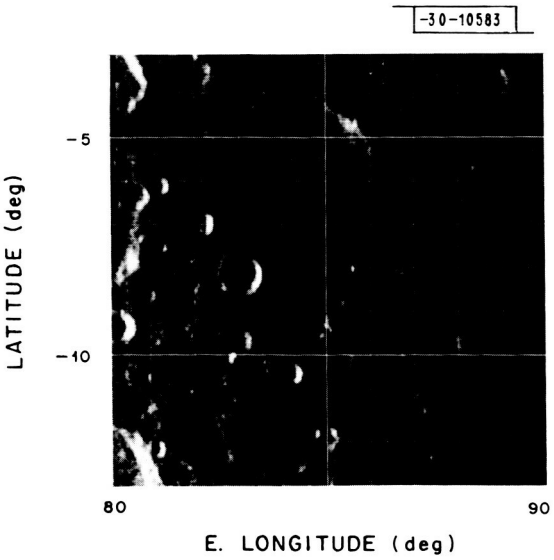

Fig. 3. Radar map of a region near eastern equatorial limb of moon in Mercator projection. Delay resolution is 10 μsec or approximately 1.5 km on surface.

II. LIMITATIONS OF SUPERSYNTHESIS TECHNIQUE

A. Introduction

In QPR (1967:1), it was demonstrated that coarse resolution maps can be constructed by combining frequency spectra obtained as the apparent libration axis of the moon rotates through 180° or more. It was suggested that the technique be applied at 23 cm to study the depolarization properties of distinctive features, and that the technique might prove helpful in constructing maps of the area near the subradar points even at 3.8 cm when the delay-Doppler technique develops difficulties.

Since that time, studies have been conducted to establish the limitations of the supersynthesis technique to determine whether it might offer the delay-Doppler technique any competition, even in the cases where beam resolution is available. Both systematic and random errors have been considered.

B. Systematic Errors

In QPR (1967:1), we showed that the filtering of the observed data with a power frequency response g(x) and the subsequent combination of the data – observed for all angles ψ between the apparent libration axis and the true lunar axis – could be interpreted as a two-dimensional convolution of the true distribution f(x, y) and a function G(x, y).

$$P(\xi;\eta) = \iint dx\,dy\; f(x,y)\; G(x-\xi,\; y-\eta) \tag{1}$$

where G(x, y) is defined by†

$$G(x,y) = 2\pi \int_0^{\infty} r\,dr \int_{-\infty}^{+\infty} d\xi\; g(\xi)\; J_0\left(2\pi r\sqrt{x^2+y^2}\right) e^{-2\pi i r\xi} \quad . \tag{2}$$

This is the complex conjugate of the result of QPR (1967:1) and in this form appears to conform better to standard practice.

This filtering of the strip distribution is equivalent to multiplying the correlation function by some weight function which de-emphasizes its values for large arguments $\sqrt{u^2+v^2}$. Let us denote this weight function by h(s) and determine its relation to the smoothing function G(x, y). The modified correlation function is $\rho_a(s\cos\psi;\; s\sin\psi) = \rho(s\cos\psi;\; s\sin\psi)\; h(s)$. This results in an expression identical to Eq. (1) except that the smoothing function is now of the form

$$G(x,y) = 2\pi \int_0^{\infty} r\,dr\; J_0\left(2\pi r\sqrt{x^2+y^2}\right) h(r) \quad . \tag{3}$$

Comparison of Eqs. (2) and (3) shows that the multiplying function h(r) is the Fourier transform of the filter function g(ρ).

As an example, we reconsider the Gaussian filter function of QPR (1967:1) where the resulting G(x, y) was quoted incorrectly because of a propagation of the 2π-error noted above. Thus,

$$g(\rho) = \exp\left[-\rho^2/2\Delta_g^2\right] \tag{4}$$

† Note the 2π in the argument of the Bessel function which was inadvertently omitted in QPR (1967:1).

gives

$$G(x, y) = \exp[-(x^2 + y^2)/2\Delta_g^2]/2\pi\Delta_g^2 \tag{5}$$

where Δ_g is the half-width of the filter.

In mapping the lunar surface as described, the filter function is given by

$$g(\rho) = \left\{\frac{\sin[\pi(\rho/\Delta_f)]}{\pi(\rho/\Delta_f)}\right\}^2 \quad . \tag{6}$$

Unfortunately, we have not yet been able to determine an analytic expression for the corresponding $G(x, y)$. However, reasonable estimates of equivalent resolution can be made by appropriate comparison with Eq. (5).

Next, it is necessary to further explore the effect of only knowing the strip distribution or the visibility function at discrete values of the angle ψ. For this purpose, we imagine that the visibility is known at N equidistant values of ψ, viz.,

$$\psi_n = \frac{\pi}{N} n \qquad n = 1, N \quad . \tag{7}$$

In addition, the complex visibility is de-emphasized at large arguments as just described. In the integral for the apparent power distribution, we therefore substitute a two-dimensional correlation function modified in the following manner:

$$\rho_a(s \cos\psi;\ s \sin\psi) = \sum_{n=0}^{N-1} \delta(\psi - \frac{\pi}{N} n)\ h(s)\ \rho(s \cos\psi;\ s \sin\psi) \quad . \tag{8}$$

Substituting Eq. (8) into that integral gives

$$P_a(x, y) = \sum_{n=0}^{N-1} \int_0^\infty s\,ds\ \{\rho(s \cos\psi_n;\ s \sin\psi_n) \exp[2\pi is(x \cos\psi_n + y \sin\psi_n)]$$

$$+ \rho^*(s \cos\psi_n;\ s \sin\psi_n) \exp[-2\pi is(x \cos\psi_n + y \sin\psi_n)\}\ h(s)$$

$$= \iint d\xi'\,d\eta'\ P(\xi';\eta') \sum_{n=0}^{N-1}$$

$$\times \int_0^\infty s\,ds\ h(s)\ 2 \cos\{2\pi s\ [(x - \xi') \cos\psi_n + (y - \eta') \sin\psi_n]\} \quad . \tag{9}$$

In this case, therefore, the two-dimensional smoothing function becomes

$$G(x, y) = 2 \sum_{n=0}^{N-1} \int_0^\infty s \cdot ds\ h(s) \cos[2\pi s(x \cos\psi_n + y \sin\psi_n)] \quad . \tag{10}$$

The particular example considered above, that of a Gaussian filter in the strip distribution, corresponds to

$$h(s) = \exp[-2\pi^2\Delta_g^2 s^2] \quad . \tag{11}$$

Substituting this into Eq. (10) gives

$$G(x, y) = 2 \sum_{n=0}^{N-1} \int_{o}^{\infty} s\, ds\, e^{-as^2} \cos(2x_n s) \tag{12}$$

where

$$a = 2\pi^2 \Delta_g^2$$

$$x_n = \pi(x \cos\psi_n + y \sin\psi_n) \quad .$$

Equation (12) can be integrated and gives†

$$G(x, y) = \frac{1}{2\pi^2 \Delta_g^2} \sum_{n=0}^{N-1} \left(1 - 2 \frac{x_n}{\sqrt{a}} \exp\{-x_n^2/a\} \int_{o}^{x_n/\sqrt{a}} e^{t^2}\, dt\right) \quad . \tag{13}$$

The function $f(y) = 1 - 2y\, e^{-y^2} \int_{o}^{y} e^{t^2}\, dt$ is shown in Fig. 4. We see from this form of G(x, y) that the contribution to G(x, y) from a particular run represented by the angle ψ_m is unity when $x_m = 0$, i.e., along a direction perpendicular to the baseline of run m. From this, it follows that the sidelobe rejection is directly proportional to the number of runs, or to the number of discrete baseline directions, as also noted in a simpler example in QPR (1967:1).

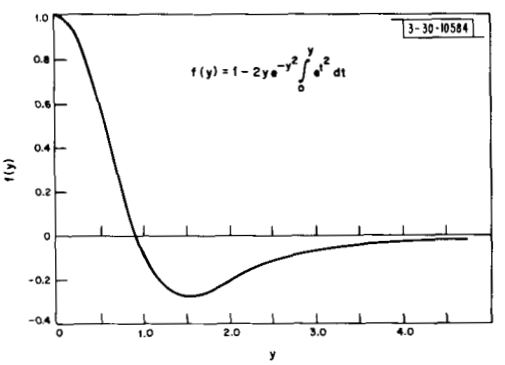

Fig. 4. Plot of function f(y).

Next consider the even more realistic case when the angle ψ is allowed to vary continuously during each observation so that the value of $\rho(u; v)$, which is assigned to a single angle ψ_m, in actual fact arises as a mean over a certain range of angles from $\psi_m - \Delta\psi/2$ to $\psi_m + \Delta\psi/2$. This form of averaging or smearing of the data occurs when the complex visibility is computed as an autocorrelation function and the instantaneous rotation axis of the target is changing direction, as in the case of lunar mapping.

When the smearing of the visibility function is caused by a rotation of the axis of the target, the modified visibility function for a particular run m becomes

† Handbook of Mathematical Functions, edited by M. Abramowitz and I.A. Stegun, Natl. Bur. Stds. Applied Math. Series 55 (1964).

$$\rho_a(s\cos\psi_m;\ s\sin\psi_m) = \iint P(\xi';\eta')\,d\xi'\,d\eta'\,\frac{1}{\Delta\psi}\int_{\psi_m-\Delta\psi/2}^{\psi_m+\Delta\psi/2} d\psi$$

$$\times \exp[-2\pi i s(\xi'\cos\psi + \eta'\sin\psi)]$$

$$= \iint P(\xi';\eta')\,d\xi'\,d\eta'\left[\frac{\sin[\pi s(\xi'\sin\psi_m - \eta'\cos\psi_m)\,\Delta\psi]}{s\pi\cdot\Delta\psi(\xi'\sin\psi_m - \eta'\cos\psi_m)}\right]$$

$$\times \exp[-2\pi i s(\xi'\cos\psi_m + \eta'\sin\psi_m)] \quad . \tag{14}$$

Introducing

$$x_n = \pi\,[(\xi' - x')\cos\psi_n + (\eta' - y')\sin\psi_n]$$

$$y_n = \pi(\xi'\sin\psi_n - \eta'\cos\psi_n)\,\Delta\psi$$

one obtains

$$G(x-\xi';\ y-\eta';\ \xi',\eta') = \sum_{n=0}^{N-1}\frac{1}{y_n}\int_o^\infty ds\ h(s)\left\{\sin\left[2s\left(x_n + \frac{y_n}{2}\right)\right] - \sin\left[2s\left(x_n - \frac{y_n}{2}\right)\right]\right\} \tag{15a}$$

and the smearing of the true distribution is no longer a true convolution. To second order in y_n,

$$G = 2\sum_{n=0}^{N-1}\int_o^\infty s\,ds\cdot h(s)\cdot\cos(2x_n s)\,(1 - s^2 y_n^2/6) \quad . \tag{15b}$$

The condition that the angular smearing of the correlation function is not to influence the data appreciably corresponds to requiring $sy_n < 1$ for all values of s for which h(s) is not close to zero. In the Gaussian case, h(s) is close to zero whenever $s > 1/\pi\cdot\Delta_g\sqrt{2}$. If r_o measured in the same units as Δ_g denotes the largest value of $\sqrt{x^2+y^2}$ in P(x, y) for which a signal is present, we conclude that the smearing is important whenever

$$\Delta\psi < \sqrt{2}\,\Delta_g/r_o \quad . \tag{16}$$

Comparison of the filter functions (4) and (6) shows that

$$\Delta_g = \Delta_f\,\frac{3}{\pi} = 0.955\,\Delta_f \quad . \tag{17}$$

As explained in QPR (1967:1), the width of the actual analyzing filter was $\Delta_f = r_o/25$ where r_o now is the lunar radius. Substitution of this into condition (16) shows that

$$\Delta\psi < \sqrt{2}\cdot 0.955/25 = 0.054 \text{ radian} = 3.1° \quad . \tag{18}$$

This is certainly <u>not</u> fulfilled in the runs analyzed in QPR (1967:1), where $\Delta\psi$ in some instances was 4°. It may be expected that the condition (16) can also be applied as a measure of the importance of the angular sampling if $\Delta\psi$ is interpreted as the angle between the libration axes on consecutive runs. In the data analyzed, this $\Delta\psi$ was as large as 10°, which seems to explain why we had to apply smoothing to the data in order to obtain a reasonable map. The contour map presented in QPR (1967:1) as Fig. 4 was obtained basically with only about 17 filters across the diameter of the moon. This sets the corresponding limit on the right-hand side of Eq. (18) at

9.3°, and satisfies the "smearing condition" as well as the "angular jump" conditions nearly throughout.

It should be added that higher resolution mapping can be achieved near the center of the moon. If we concentrate our attention only on the central disk to $r_o = \frac{1}{2}$, then condition (16) can be satisfied with larger values of $\Delta\psi$. We reanalyzed the data of 27 and 28 December 1966 with essentially 31 filters across the lunar diameter, and the result is shown in Fig. 5. The sidelobe level along the edges is very prominent, as the above analysis predicts. However, it appears that the resolution is considerably increased near the center. It is particularly interesting to note how Copernicus has emerged as a distinct separate feature on this scale [see Fig. 5 and compare with Fig. 4 in QPR (1967:1)].

C. Random Errors

Random errors in the estimate of the reflectivity in the maps arise either because there is an appreciable amount of random additive noise superimposed on the signal, or because the signal itself fades so that the mean signal power even in the absence of additive noise may only be determined after a certain amount of signal integration. For most radar astronomy targets, except for the moon, additive noise is of greatest importance. When the most sensitive radar systems are applied to the study of the moon, however, the returns are so strong that additive noise is not the limiting factor. For this reason, we shall discuss the latter case.

It is difficult to give a completely general discussion of the computation of the random errors covering all experimental situations. Thus, we shall consider the particular experimental situation which arises in lunar observations where as an approximation one may regard the projection of the instantaneous apparent axis to rotate at a constant angular velocity $\dot{\psi}$. We shall also assume that the rotation rate $|\vec{\Omega}|$ (and hence the limb-Doppler) remains constant. The observation will be assumed to be carried out continuously so that problems in connection with discrete angular sampling do not arise. (The experiment is therefore highly idealized.) The angle ψ must be replaced by $\dot{\psi}t$, where t is the time, and the variable s [e.g., see Eq. (8)] will be replaced by $2\tau\Omega_{||}/\lambda$, where τ is the time shift in the correlation function and $\Omega_{||}$ is the projection of the apparent angular velocity on the x, y plane. For the time-varying autocorrelation function at time t and delay τ, one obtains

$$\rho(\tau; t) = \iint dx\,dy\; P(x;y)\; \exp\left[-4\pi i\,\frac{\tau}{\lambda}\,\Omega_{||}\,\{x\,[\cos\psi t\cdot(\dot{\psi}\tau/2) - \sin\psi t] + y\,[\sin\psi t\cdot(\dot{\psi}\tau/2) + \cos\psi t]\}\right] \quad . \tag{19}$$

As explained previously, this ideal correlation function must be multiplied by a weight function $h(\tau)$ in order to achieve some filtering of the data. Furthermore, we cannot arrive at an estimate of the instantaneous correlation function at time t. In practice, we must make an estimate by taking a time average. Therefore, the correlation function available for transformation will be a random variable having a mean value given by

$$\rho_m(\tau; t) = h(\tau) \int_{-\infty}^{+\infty} \rho(\tau, t')\; g(t - t')\; dt' \tag{20}$$

where $g(t)$ is a time-averaging function. The estimate of the filtered brightness over the target disk is

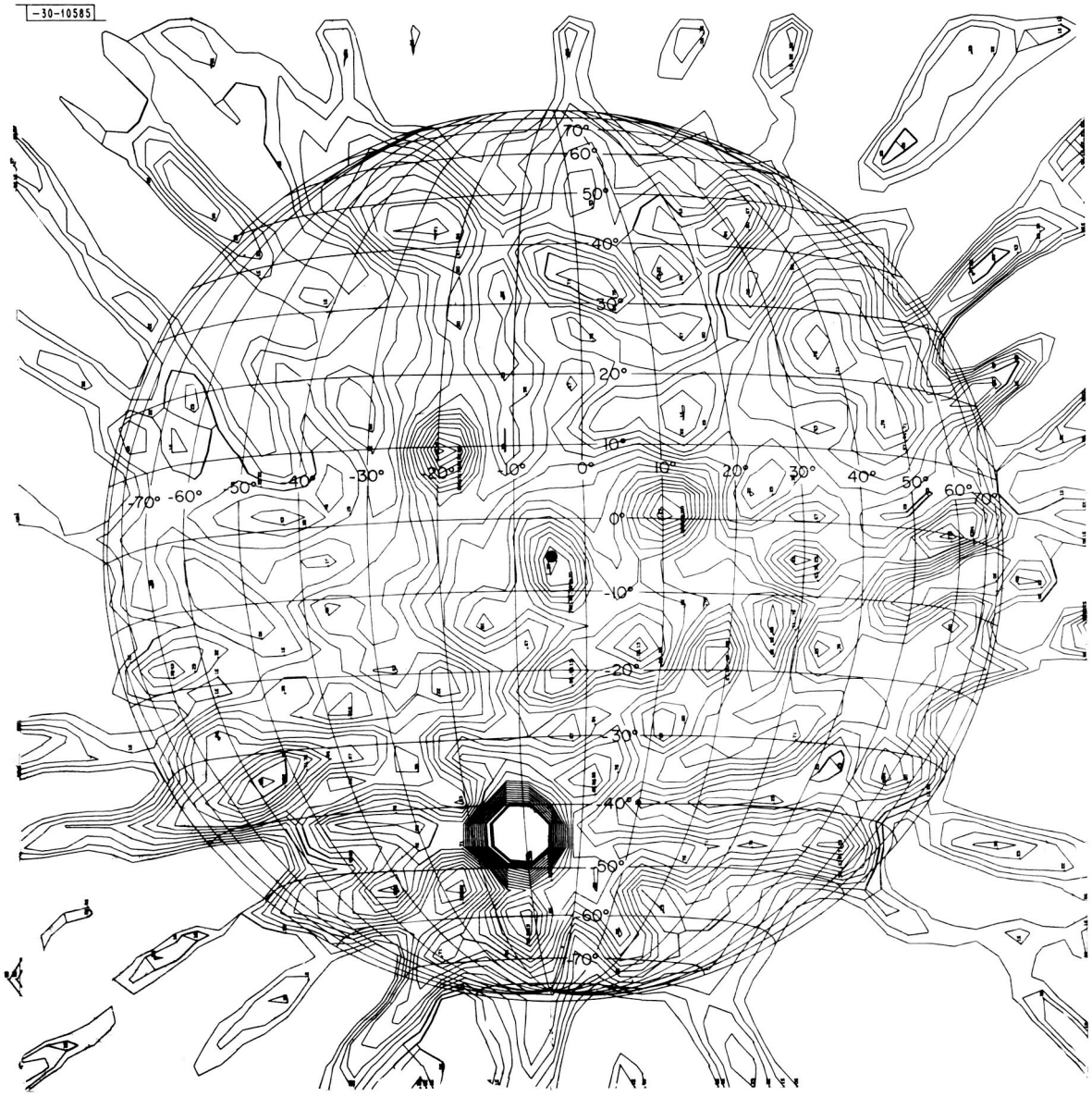

Fig. 5. Contour map of lunar reflectivity, depolarized circular component, 23-cm wavelength. Contours labeled in relative power. Filt = 0.132.

$$P_m(x;y) = \kappa \iint d\tau\, dt\, \tau \rho_m(\tau;t) \exp[4\pi i \frac{\tau}{\lambda} \Omega_{||}(x \cos\psi t + y \sin\psi t)] \tag{21}$$

where κ is a constant of proportionality. Here, $\rho_m(\tau;t)$ is to be considered the mean value of the random variable $\rho_m^i(\tau;t)$; hence,

$$\rho_m(\tau;t) = \langle \rho_m^i(\tau;t) \rangle \quad .$$

The deviation or uncertainty in $P_m(x;y)$ is given by

$$\delta P_m^i(x,y) = \kappa \iint d\tau\, dt\, \tau(\rho_m^i - \rho_m) \exp[4\pi i \frac{\tau}{\lambda} \Omega_{||}(x \cos\psi t + y \sin\psi t)] \tag{22}$$

and the mean-square uncertainty becomes

$$\delta P_m(x,y)^2 = \langle \delta P_m^i(x,y)^2 \rangle = \kappa^2 \iiiint d\tau\, dt\, d\tau'\, dt' \, (\langle \rho_m^i \rho_m^{i*'} \rangle - \rho_m \rho_m^{*'})\, \tau\tau'$$
$$\times \exp\{\frac{4\pi i}{\lambda} \Omega_{||} [\tau(x \cos\psi t + y \sin\psi t) - \tau'(x \cos\psi t' + y \sin\psi t')]\} \tag{23}$$

the primed functions having arguments τ' and t'. In order to compute the mean of the product of "instantaneous correlation functions" appearing under the integral sign, we proceed as follows:

$$\langle \rho_m^{i*}(\tau';t')\, \rho_m^i(\tau;t) \rangle = h(\tau)\, h(\tau') \iint dt''\, dt'''\, g(t - t'')\, g(t' - t''')$$
$$\cdot \langle \rho^i(\tau;t'')\, \rho^{i*}(\tau';t''') \rangle \quad . \tag{24}$$

Since the random variable $\rho^i(\tau;t)$ is defined as a simple product of two random variables which are nearly always Gaussian, we may express the mean of the product in Eq. (24) in terms of products of means

$$\begin{aligned}
\langle \rho^i(\tau;t'')\, \rho^{i*}(\tau';t''') \rangle &= \langle f^*(t''+\tau)\, f(t'')\, f(t'''+\tau')\, f^*(t''') \rangle \\
&= \langle f^*(t''+\tau)\, f(t'') \rangle \langle f(t'''+\tau')\, f^*(t''') \rangle + \langle f^*(t''+\tau)\, f(t'''+\tau') \rangle \\
&\quad \cdot \langle f(t'')\, f^*(t'') \rangle \\
&= \rho(\tau;t'')\, \rho^*(\tau';t''') + \rho^*(\tau' - \tau + t''' - t'';\ t''+\tau) \\
&\quad \times \rho(t''' - t'';\ t'') \quad .
\end{aligned} \tag{25}$$

The former of these two terms will only serve to cancel the product of the means in Eq. (23) and there remains

$$\delta P_m(x,y)^2 = \kappa^2 \int \cdots \int d\tau\, d\tau'\, dt\, dt'\, \tau\tau' \exp\{\frac{4\pi i}{\lambda} \Omega_{||} [\tau(x \cos\psi t + y \sin\psi t)$$
$$- \tau'(x \cos\psi t' + y \sin\psi t')]\} \times h(\tau)\, h(\tau') \iint dt''\, dt'''\, g(t - t'')$$
$$\times g(t' - t''')\, \rho^*(\tau' - \tau + t''' - t'';\ t''+\tau)\, \rho(t''' - t'';\ t'') \quad . \tag{26}$$

This expression is so complex that general conclusions cannot easily be drawn regarding the relative uncertainty in the reflectivity determinations. Under these circumstances, the best one can accomplish apparently is to construct an example which is simple enough for the computations to be carried through, yet complex enough to convey information of general validity. It appears that the following distribution is of such a nature:

$$P(x; y) = \exp[-(x^2 + y^2)/2a^2] \tag{27}$$

where a is a measure of the extent of the moon. From Eq. (19), it follows that

$$\rho(\tau; t) = \exp\{-2\pi^2(\tau f_L)^2 [1 + (\psi\tau/2)^2]\} \approx \exp[-2\pi^2(\tau f_L)^2] \quad . \tag{28}$$

Here we have introduced $f_L = 2a\Omega_{||}/\lambda$, which corresponds to the "limb-Doppler" of a planet of radius a. Since $\rho(\tau; t)$ is not dependent on t, the convolution with $g(t - t')$ in Eq. (20) has no effect. Using a Gaussian weight factor $h(\tau)$ as in Eq. (11), one obtains

$$\rho_m(\tau, t) = \exp\{-2\pi^2(f_L\tau)^2 [1 + (\Delta_g/f_L)^2]\} \cong e^{-\beta^2\tau^2} \quad . \tag{29}$$

Substituting this into Eq. (21) gives

$$P_m(x; y) = \frac{\kappa}{\dot{\psi}} \int_0^\infty \tau\, d\tau\, d^{-\beta^2\tau^2} \int_0^\pi d\varphi\, \exp[4\pi i \frac{\tau}{\lambda} \Omega_{||}(x \cos\varphi + y \sin\varphi)]$$

$$= \frac{\pi\nu}{\dot{\psi}} \int_0^\infty \tau\, d\tau\, e^{-\beta^2\tau^2} J_0(4\pi\sqrt{x^2 + y^2} \frac{\tau}{\lambda} \Omega_{||})$$

$$= \frac{\kappa}{4\pi\dot{\psi} f_L^2 [1 + (\Delta_g^2/f_L^2)]} \exp\left\{-\frac{x^2 + y^2}{2a^2 [1 + (\Delta_g^2/f_L^2)]}\right\} \quad . \tag{30}$$

The mean observed distribution is therefore seen to closely resemble the original distribution as long as $\Delta_g << f_L$.

In order to compute the uncertainty $\delta P_m(x, y)$, we have to make the additional assumption that

$$g(t - t') = \frac{1}{\sqrt{2\pi}\, T_o} \exp[-(t - t')^2/2T_o^2] \quad . \tag{31}$$

With this assumption we find, after some considerable labor, that

$$\langle \rho_m^i \rho_m^{i*'} \rangle - \rho_m \rho_m^{*'} = \frac{1}{\sqrt{3 + 2(2\beta T_o)^2}} \exp[-\alpha^2(\tau^2 + \tau'^2)] \cdot \exp[-(\beta/2)\, \Delta\tau^2]$$

$$\cdot \exp\left\{-\frac{1}{2T_o^2}\left[\frac{2 + (2\beta T_o)^2}{3 + 2(2\beta T_o)^2}\right] (t - t' - \frac{\Delta\tau}{2})^2\right\} \tag{32}$$

where $\Delta\tau = \tau' - \tau$, and $\alpha = \sqrt{2\pi}\, \Delta_g$. We note that $\beta T_o \cong \sqrt{2\pi}\, f_L \cdot T_o$. The duration of a fading cycle is typically f_L^{-1}. Since T_o must include a great many fading cycles, we conclude that $\beta T_o >> 1$. For the same reason, $\Delta\tau$ can be ignored in the last exponential factor by putting $\Delta\tau = 0$. We also note that $\alpha << \beta$ for reasonable resolution to be obtained. It follows that, in the first exponential factor one may put $\tau = \tau'$. With these simplifications, one obtains

$$\langle \rho_m^i \rho_m^{i*'} \rangle - \rho_m \rho_m^{*'} \approx \frac{1}{\sqrt{2}\, 2\beta T_o} \exp\left[-2\alpha^2\tau^2 - \frac{\beta^2}{2} \Delta\tau^2 - \frac{1}{4T_o^2} \Delta t^2\right] \tag{33}$$

with $\Delta t = t' - t$.

When substituting into Eq. (23), we expand the exponent of the phase factor to first order in Δt about $\Delta t = 0$ and integrate with respect to t. The result is

$$\frac{\pi\kappa^2}{\sqrt{2}\,\psi\beta T_o}\int_o^\infty \tau\,d\tau\cdot e^{-\alpha^2 2\tau^2}\int_{-\tau}^{\infty} d(\Delta\tau)\,(\tau+\Delta\tau)\cdot e^{-\beta^2\Delta\tau^2/2}$$

$$\cdot\int_{-\infty}^{+\infty} d(\Delta t)\cdot e^{-\Delta t^2/4T_o^2}\cdot J_o\left[2\pi f_L\frac{r}{a}\sqrt{\Delta\tau^2+\tau^2(\dot\psi\Delta t)^2}\right] = \delta P_m(r)^2 \qquad (34)$$

where $r = \sqrt{x^2+y^2}$. Since this is not easily integrable, we have to be content to find an upper bound to $\delta P_m(r)^2$ by computing the triple integral for $r = 0$ only. Making some further approximations which are all compatible with previous assumptions, we finally obtain

$$\delta P_m^2 \leqslant \frac{\pi}{4}\left(\frac{\pi}{2}\right)^{3/2}\frac{\kappa^2}{\dot\psi\beta^2\cdot\alpha^3} \quad . \qquad (35)$$

Substitution of $\dot\psi = \pi/T$, where T is the total time of observation, and computation of the relative uncertainty gives for $r = 0$

$$\frac{\delta P_m^2}{P_m^2} \approx \frac{\sqrt{\pi}}{4}\cdot\frac{1}{T\Delta_g}\cdot\left(\frac{f_L}{\Delta_g}\right)^2 \quad . \qquad (36)$$

We note that this is independent of transmitter power because of the absence of additive noise. The uncertainty $\delta P_m/P_m$ is inversely proportional to the square root of observation time multiplied by the smoothing filter bandwidth, and directly proportional to linear resolution. For a given resolution, we see that the uncertainty is inversely proportional to the square root of the operating frequency since, for a given resolution, one must make $\Delta_g \sim$ operating frequency.

Suppose we desire to obtain reflectivity data to an accuracy of $\delta P_m/P_m = 0.25$. Let us determine, according to Eq. (36), to what resolution we can map. Taking 12 hours as a typical observing time and the limb-Doppler to be 10 Hz, one obtains

$$\frac{\Delta_g}{f_L} \geqslant 2.54\cdot 10^{-2}$$

which corresponds to a resolution of 43 km on the moon. This appears to be the ultimate resolution which the method can yield at 23 cm using the Millstone antenna. At 3.8 cm where the narrow antenna beam can be used to effectively reduce the apparent size of the moon, the achievable resolution for the same relative uncertainty should be about one-tenth of this, i.e., approximately 5 km. In view of the excellent resolution achieved – even near the subradar point – in the delay-Doppler technique at 3.8 cm using the Haystack antenna, it does not appear worthwhile to implement the supersynthesis technique for high-resolution mapping of the moon at 3.8 cm. However, for further detailed polarization studies of the moon at 23 cm, the method appears to be valuable.

III. PROGRESS WITH 8-MM RADAR SYSTEM

During this quarter, the 1-kW 35-GHz klystron amplifier tube was delivered and is now operating on the bench at 1.2 kW. The transmitter assembly for this high-power tube is completed and is operating smoothly. The control logic and remote monitoring equipment are nearly

finished. A thermal detuning problem, which at the moment prevents stable operation, has been encountered but is not expected to impede the progress. The oscillator and multiplier chain for the tube also seem to work satisfactorily.

Because of delay in delivery of the kilowatt tube, considerable time has been spent on the 50-W transmitter. The original method of phase-locking the 35-GHz klystron oscillator in this transmitter has proven to be excessively inconvenient. Now the 50-W tube can be phase-locked provided the reference frequency is correct. The tube will only oscillate at a frequency determined by uncontrollable internal tube parameters. For this reason, the reference frequency has had to be supplied by means of a spectrum of crystals. A different and much more convenient reference frequency synthesizer has now been implemented and is currently being installed in the radar cab. Its primary purpose is to provide a reference frequency which can be readily adjusted so that the 35-GHz klystron is locked at a frequency at which it oscillates strongly.

The remainder of the millimeter effort has progressed in a more satisfying manner. The new rate drives for pointing the antenna are strikingly successful. Installation of encoders on the azimuth and elevation shafts is nearly completed. The pointing and Doppler data are now being supplied by the CDC-3300 Haystack computer on a regular schedule and in convenient form.

Returns from the moon have been observed during this reporting period but, to date, the Doppler correction has not been working satisfactorily. With the new frequency control system described above, this difficulty is expected to disappear so that reflectivity data may be obtained using the 50-W tube.

ACKNOWLEDGMENTS

The work of most of the technical personnel of Group 31, Surveillance Techniques, which operates the facilities of the Field Station, in preparing and conducting the work reported to date is gratefully acknowledged, as is the work of members of Group 46, Microwave Components, in cooperating with Dr. McCue on the 8.6-mm radar.

The use of the facilities of the Lincoln Laboratory Millstone-Haystack complex, provided by the U.S. Air Force, is also gratefully acknowledged.